Letters

A Clamp Circuit-Based Inductive Power Transfer System With Reconfigurable Rectifier Tolerating Extensive Coupling Variations

Yang Chen, *Senior Member, IEEE*, Zeheng Zhang, Bin Yang, Binshan Zhang, Ling Fu, Zhengyou He, *Senior Member, IEEE*, and Ruikun Mai, *Senior Member, IEEE*

***Abstract*—Coupling variation tolerance is one of the most crucial abilities of the inductive power transfer (IPT) system because the variable coupling can dramatically degrade the output power. This letter proposes a clamp circuit-based IPT system with a reconfigurable rectifier featuring high antimisalignment. The clamp circuit can adaptively switch from one stable operating region to the other according to the coupling coefficients. The reconfigurable rectifier can work in half-bridge mode or full-bridge mode, which can build another two adaptively switching stable operating regions such that the proposed IPT system can provide nearly stable output power resisting extensive coupling variations. A 400-W prototype was built to verify the theoretical analysis. The experimental results indicate that the output power fluctuation of the proposed method is only 5.98% when the coupling coefficient varies from 0.1 to 0.4 (400%), and the system efficiency is from 86.1% to 94.3%. The proposed method does not need complicated control or dedicated coil design, and it can implement significant antimisalignment improvement.**

***Index Terms*—Clamp circuit, coupling variation, inductive power transfer (IPT), reconfigurable rectifier.**

I. Introduction

FLEXIBILITY is one of the attractive features of inductive power transfer (IPT) since the position of the secondary coil is frequently arbitrary [1], [2]. It can bring a large coupling variation to the IPT system, leading to a reduction in transferred power. Therefore, the IPT system should be equipped with the crucial ability of misalignment tolerance.

Current preferred solutions for maintaining relatively stable output power mainly include coil design and compensation topology so the IPT system can have the inherent coupling-insensitive capability. In coil design, the double-D coil [3], solenoid coil [4], and antiparallel windings [5], [6] are optimized to build a relatively uniform magnetic field for the secondary coil. However, these methods widely rely on strict design requirements, and most of them only tolerate vertical or horizontal offset. Besides, the hybrid compensation topology integrated with two topologies, which have opposite trends in outputs versus coupling, can improve misalignment tolerance [7]. The integrations can be S–S and *LCC*–*LCC* topologies [8] or *LCC*-S and S-*LCC* topologies [9]. Nevertheless, they require many passive components, and the allowable misalignment directions are limited. For a compensation topology, the transfer power versus coupling coefficient (P–k) curve is determined once the parameters are fixed. If the parameters of the compensation topologies, such as X-S [10], S-S [11], *LCC*-S [12], and S-SP [13], are specifically detuned, the top region of the P–k curve can be relatively stable. To enhance the coupling variation tolerance, a reconfigurable topology based on detuned compensation is proposed to create a new P–k curve, so the top region is extended [14]. Nevertheless, the output power fluctuation is about 10% against a 250% coupling variation. It would be much better if the power drop is further reduced with a more extensive coupling variation range.

This letter proposes a clamp circuit-based IPT system with a reconfigurable rectifier that tolerates significant coupling variations. The clamp circuit enables two P–k curves with stable top regions owning adaptively switching according to the coupling factor, and the reconfigurable rectifier altering from the half-bridge mode (HBM) to the full-bridge mode (FBM) results in the right shift of the two P–k curves such that the proposed IPT system features highly robust power transfer versus significant variations of the coupling coefficient. The experimental results with a 400-W prototype are presented to demonstrate the misalignment performances of the proposed method.

II. Theoretical Analysis

A. System Topology

Fig. 1 depicts the proposed clamp circuit-based IPT system with a reconfigurable rectifier. U_p (U_s) and I_p (I_s) are the high-frequency input (output) voltage and current of the S–S topology. L_p (L_s) and C_p (C_s) are the primary (secondary) coil and compensation capacitor. R_{ac} is the equivalent ac load. The

Manuscript received 9 May 2023; revised 21 July 2023; accepted 6 August 2023. Date of publication 9 August 2023; date of current version 22 December 2023. This work was supported in part by the National Natural Science Foundation of China under Grant 52207226 and in part by Sichuan Science and Technology Program under Grants 2023NSFSC0819 and 2023JDRC0102. *(Corresponding author: Ling Fu.)*

The authors are with the Key Laboratory of Magnetic Suspension Technology and Maglev Vehicle, Ministry of Education, Chengdu 611756, China, and also with the School of Electrical Engineering, Southwest Jiaotong University, Chengdu 611756, China (e-mail: yangchen@swjtu.edu.cn; hengs@my.swjtu.edu.cn; yb@my.swjtu.edu.cn; zbs@my.swjtu.edu.cn; lingfu@swjtu.edu.cn; hezy@home.swjtu.edu.cn; mairk@swjtu.edu.cn).

Color versions of one or more figures in this article are available at https://doi.org/10.1109/TPEL.2023.3303487.

Digital Object Identifier 10.1109/TPEL.2023.3303487

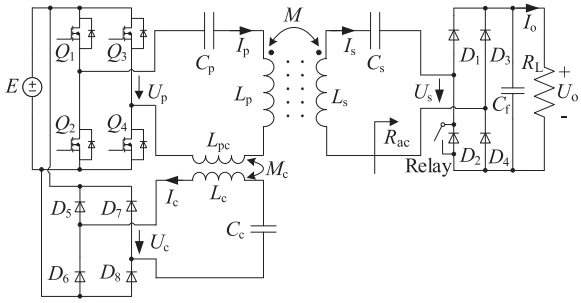

Fig. 1. Proposed clamp circuit-based IPT system with a reconfigurable rectifier.

clamp circuit consists of a diode rectifier (D_5–D_8), a compensation element C_c, and a clamp transformer, where L_{pc}, L_c, and M_c are the self-inductances and mutual inductance. A capacitor, for convenience, is used to represent the compensation element C_c, which can be a capacitor or an inductor determined by its parameter value. The reconfigurable rectifier is formed by a diode rectifier (D_1–D_4) and a relay for reconfiguring purposes. Four MOSFETs (Q_1–Q_4) compose the high-frequency inverter, and the relationship between input dc voltage E and U_p is expressed as follows:

$$E = \sqrt{2}\pi U_p/4. \tag{1}$$

The secondary capacitor C_s is designed to fully compensate the secondary coil L_s, so we have

$$jX_s = j\omega L_s + 1/(j\omega C_s) = 0 \tag{2}$$

where ω is the angular frequency.

The impedances of the primary and the clamp loops are given as

$$\begin{cases} X_p = X_{Lp} - X_{Cp} + X_{Lpc}, X_M = k\sqrt{X_{Lp}X_{Ls}} \\ X_c = X_{Lc} - X_{Cc},\ X_{Mc} = \omega M_c \end{cases} \tag{3}$$

where $X_{Lp}=\omega L_p$, $X_{Cp}=1/\omega C_p$, $X_{Lpc}=\omega L_{pc}$, $X_{Lc}=\omega L_c$, $X_{Cc}=1/\omega C_c$, and k is the coupling coefficient.

B. Working Principle of the Clamp Circuit

If the primary current I_p is not so large, the amplitude of U_c will not exceed the input dc voltage E, which means the clamp circuit is regarded as not conductive [15], and the system operating as a detuned S–S topology can be described as follows:

$$\begin{bmatrix} U_p \\ 0 \end{bmatrix} = \begin{bmatrix} jX_p & -jX_M \\ -jX_M & jX_s + R_{ac} \end{bmatrix} \begin{bmatrix} I_p \\ I_s \end{bmatrix}. \tag{4}$$

Substituting (3) into (4), the output power P_s of the system can be derived as follows:

$$P_s = \frac{R_{ac}X_{Lp}X_{Ls}U_p^2k^2}{X_p^2R_{ac}^2 + (X_{Lp}X_{Ls}k^2)^2} = P_s(k) \tag{5}$$

which demonstrates that the output power can be treated as a function of coupling coefficient k ($0 < k < 1$), namely, $P_s(k)$.

By setting the derivative of $P_s(k)$ to 0, i.e., $P_s'(k) = dP_s(k)/dk = 0$, we can obtain an inflection point $k_{\inf}$

$$k_{\inf} = \sqrt{\frac{X_pR_{ac}}{X_{Lp}X_{Ls}}}. \tag{6}$$

The output power can reach the maximum value $P_{s\max}$ at the inflection point, namely

$$P_{s\max} = \frac{U_p^2}{2X_p}. \tag{7}$$

There is an induced voltage $U_{\mathrm{ind}\,c}$ in the clamp circuit, and $|U_{\mathrm{ind}c}|$ can be derived as follows:

$$|U_{\mathrm{ind}c}| = \frac{U_pX_{Mc}R_{ac}}{\sqrt{X_p^2R_{ac}^2 + X_{Lp}^2X_{Ls}^2k^4}}. \tag{8}$$

According to (8), when the coupling k decreases, the induced voltage will become larger. If the amplitude of U_c exceeds the input dc voltage E, the clamp circuit is partly conductive, where the current I_c is relatively small, and the system still can be considered as an S–S topology [15].

When the amplitude of U_c further increases to more than $4E/\pi$, the clamp circuit is regarded as conductive, in that case, the system is described as

$$\begin{bmatrix} U_p \\ 0 \\ U_p \end{bmatrix} = \begin{bmatrix} jX_p & -jX_M & jX_{Mc} \\ -jX_M & jX_s + R_{ac} & 0 \\ jX_{Mc} & 0 & jX_c \end{bmatrix} \begin{bmatrix} I_p \\ I_s \\ I_c \end{bmatrix}. \tag{9}$$

Substituting (3) into (9), the output power P_{sc} of the system is given as

$$P_{sc} = \frac{R_{ac}X_{Lp}X_{Ls}U_p^2k^2(X_c - X_{Mc})^2}{(X_{Mc}^2 - X_pX_c)^2R_{ac}^2 + (X_cX_{Lp}X_{Ls}k^2)^2} = P_{sc}(k). \tag{10}$$

Similarly, we can acquire an inflection point $k_{\inf c}$, where the output power can reach the maximum value $P_{s\max c}$, i.e.,

$$k_{\inf c} = \sqrt{\frac{(X_pX_c - X_{Mc}^2)R_{ac}}{X_cX_{Lp}X_{Ls}}} \tag{11}$$

$$P_{s\max c} = \frac{U_p^2(X_c - X_{Mc})^2}{2X_pX_c^2 - 2X_cX_{Mc}^2}. \tag{12}$$

According to the above-mentioned analysis, the P–k curves of the clamp circuit-based IPT system can be roughly outlined in Fig. 2. Letting $P_s(k) = P_{sc}(k)$, there is an intersection at k_{int} of the two curves and corresponding values are listed as

$$k_{\mathrm{int}} = \sqrt{\frac{R_{ac}(X_{Mc} - X_p)}{X_{Lp}X_{Ls}}} \tag{13}$$

$$P_{s\mathrm{int}} = \frac{(X_{Mc} - X_p)U_p^2}{2X_p^2 - 2X_pX_{Mc} + X_{Mc}^2}. \tag{14}$$

Letting the maximum values of the two curves be equal, i.e., $P_{s\max} = P_{s\max c}$, we can obtain

$$X_c = \frac{X_pX_{Mc}}{2X_p - X_{Mc}}. \tag{15}$$

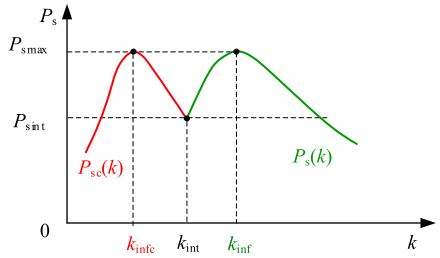

Fig. 2. *P–k* curves of the clamp circuit-based IPT system.

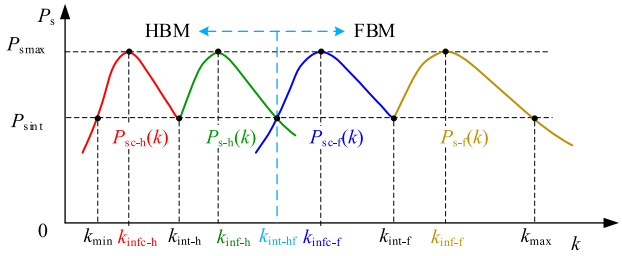

Fig. 3. *P–k* curves of the clamp circuit-based IPT system with a reconfigurable rectifier.

It can be found that the clamp circuit-based IPT system can adaptively switch from one *P–k* curve to the other *P–k* curve according to the coupling coefficients such that the stable output region is expanded.

C. Working Principle of the Reconfigurable Rectifier

Unless otherwise stated, subscripts $-h$ and $-f$ indicate the HBM and FBM. The reconfigurable rectifier has two working modes [16]. When the relay is ON, the reconfigurable rectifier works in HBM, and the corresponding ac load $R_{ac\text{-}h}$ is $R_{ac\text{-}h} = (2/\pi^2)R_L$. When the relay is OFF, it operates in FBM, and the ac load $R_{ac\text{-}f}$ satisfies $R_{ac\text{-}f} = (8/\pi^2)R_L$, so we have $R_{ac\text{-}f} = 4R_{ac\text{-}h}$. Therefore, the reconfigurable rectifier can alter the ac load from one value to the other.

Based on (6) and (11), if the ac load increases, the two *P–k* curves will shift to the right, as shown in Fig. 3. Likewise, letting $P_{s\text{-}h}(k) = P_{sc\text{-}f}(k)$, there is an intersection at $k_{int\text{-}hf}$ of the two power curves and the corresponding values are derived as

$$k_{int-hf} = \sqrt{\frac{2R_{ac-h}\left(X_{Mc} - X_p\right)}{X_{Lp}X_{Ls}}} \tag{16}$$

$$P_{sint-hf} = \frac{2\left(X_{Mc} - X_p\right)U_p^2}{5X_p^2 - 8X_pX_{Mc} + 4X_{Mc}^2}. \tag{17}$$

Letting the output power P_{sint} at $k_{int\text{-}h}$ and the output power $P_{sint\text{-}hf}$ at $k_{int\text{-}hf}$ be equal, i.e., $P_{sint} = P_{sint\text{-}hf}$, we can have

$$X_p = \left(2 - \sqrt{2}\right)X_{Mc}. \tag{18}$$

If the parameters are appropriately designed, the system can operate at the top regions of the *P–k* curves with a relatively small power fluctuation tolerating a large coupling variation. When the coupling coefficient k is located in $[k_{min}, k_{int\text{-}hf}]$, the reconfigurable rectifier works in HBM; when the coupling coefficient k belongs to $[k_{int\text{-}hf}, k_{max}]$, the FBM operates.

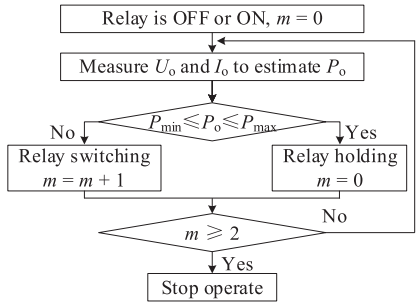

Fig. 4. Flowchart of the relay control.

The flowchart of the relay control is described in Fig. 4. The output voltage U_o and current I_o are measured to evaluate the output power P_o. By comparing the estimated P_o with the maximum and minimum power (P_{max} and P_{min}), the controller determines whether the relay should turn ON or OFF. If the output power does not satisfy the required power after the operation of the relay ($m \geq 2$), the system should be stopped since the coupling is beyond the variation range.

D. Parameter Design

In order to design the system parameters, some parameters should be given first, including ω, L_p, L_s, $k_{int\text{-}hf}$, P_{smax}, and R_L.

Then, substituting (18) into (16), X_{Mc} can be yielded as

$$X_{Mc} = \frac{\pi^2 X_{Lp}X_{Ls}k_{inf-hf}^2}{4\left(\sqrt{2}-1\right)R_L}. \tag{19}$$

Combined with (19) and (18), X_p is given as

$$X_p = \frac{\sqrt{2}\pi^2 X_{Lp}X_{Ls}k_{inf-hf}^2}{4R_L}. \tag{20}$$

Afterward, substituting (19) and (20) into (15), X_c is obtained as

$$X_c = \frac{\left(4+3\sqrt{2}\right)\pi^2 X_{Lp}X_{Ls}k_{inf-hf}^2}{4R_L}. \tag{21}$$

Equations (19)–(21) present the key parameters of the proposed IPT system, and the values of the components can be acquired according to (1), (3), and (7).

III. Experimental Validation

A. Experimental Results

A 400-W experimental prototype, as shown in Fig. 5, is constructed to validate the feasibility of the proposed approach. The system parameters of the prototype are tabulated in Table I. For the component element C_c, it turns out to be an inductor calculated by (21) and (3), such that C_c is treated as one inductor together with L_c.

Steady-state experimental waveforms of the output current/voltage of the inverter and the input current/voltage of the two rectifiers with different coupling factors are captured for

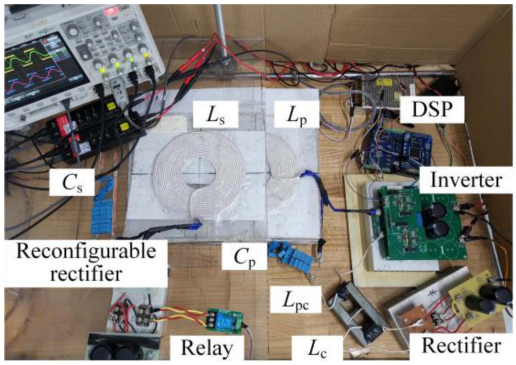

Fig. 5. Schematic diagram of the experimental prototype.

TABLE I
IPT SYSTEM SPECIFICATION AND PARAMETER VALUES

Parameter	Value	Parameter	Value
E	120 V	ω	2π×200 kHz
L_p	37.83 μH	L_s	37.29 μH
C_p	15.75 nF	C_s	16.98 nF
L_{pc}	12.65 μH	L_c	57.29 μH
M_c	16.66 μH	P_{smax}	400 W
$k_{int\text{-}hf}$	0.2	R_L	24 Ω

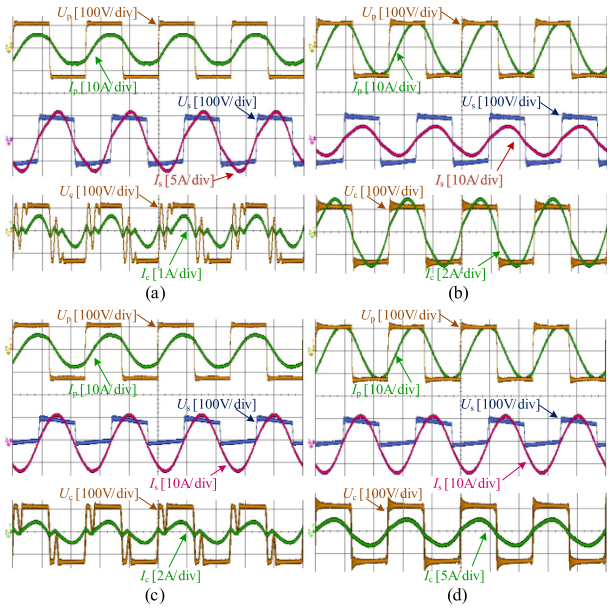

Fig. 6. Experimental waveforms of U_p, I_p, U_s, I_s, U_c, and I_c. (a) $k = 0.39$ in FBM. (b) $k = 0.22$ in FBM. (c) $k = 0.18$ in HBM. (d) $k = 0.11$ in HBM.

the FBM and HBM, respectively, as given in Fig. 6. In the FBM with $k = 0.39$, the current I_c is relatively small and thereby the clamp circuit is partly conductive, as shown in Fig. 6(a). With the decrease of coupling factor, the clamp circuit is fully conductive, as shown in Fig. 6(b), where $k = 0.22$. In the HBM, as shown in Fig. 6(c) and (d), we can observe some similar situations. Besides, the current I_s of the reconfigurable rectifier is almost doubled to keep the output power nearly constant because the voltage U_s is halved when the mode is altered from FBM to HBM.

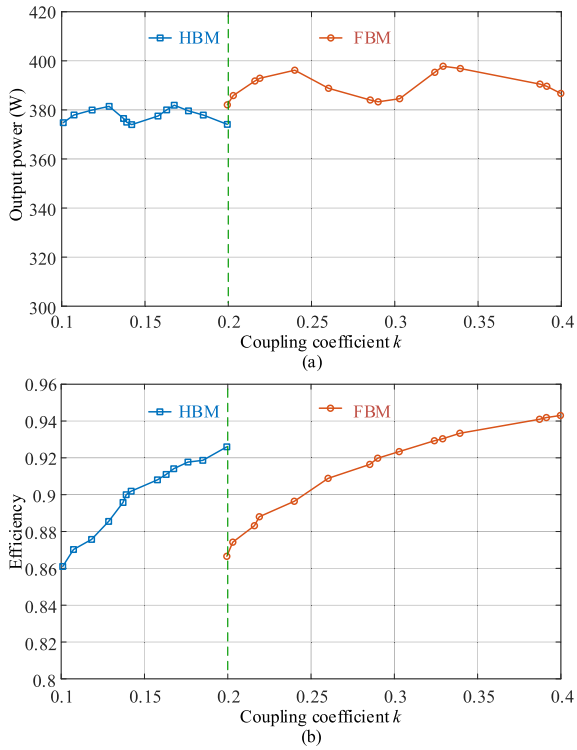

Fig. 7. Experimental results of the (a) output power and (b) efficiency of the system with coupling variations.

The transferred power and corresponding system efficiency from dc to dc with different coupling coefficients are outlined in Fig. 7. When the coupling factor locates in [0.2, 0.4], the IPT system operates in FBM, when the maximum power is about 397.8 W, and the minimum value is around 383.3 W. When the coupling range is [0.1, 0.2], the half-bridge rectifier is active, and the maximum and minimum power is about 381.9 W and 374.0 W, respectively. It can be observed that the output power in HBM is a little lower than that in FBM, which is due to the effects of the series equivalent resistance in the circuit and tolerance of the system parameters. However, with the coupling factor varying from 0.1 to 0.4, the power fluctuation of the IPT system is only (397.8–374.0)/397.8 = 5.98%, demonstrating that the proposed method can tolerate an extremely large coupling variation with a slight power fluctuation. The measured efficiency versus coupling coefficient is plotted in Fig. 7(b). The efficiency of the IPT system in FBM is [87.4%, 94.3%] within the coupling range of [0.2, 0.4], while the efficiency in HBM is [86.1%, 92.6%] when the coupling belongs to [0.1, 0.2].

B. Discussion and Comparison

It should be emphasized that the proposed method differs from [15], the idea of which is only to realize the self-adaptive CC–CV charging for the battery based on the clamp circuit under resonant conditions. However, this work is to achieve extremely high-misalignment tolerance for the IPT system using a clamp circuit and reconfigurable rectifier under detuned conditions. The main contributions and implementation methods of these two works are quite different.

TABLE II
COMPARISON WITH OTHER METHODS REPORTED IN THE LITERATURE

Literature	[7]	[8]	[9]	[10]	[11]	[12]	[13]	[14]	This work
Operating frequency	85 kHz	85 kHz	85 kHz	200 kHz	200 kHz	140 kHz	200 kHz	250 kHz	200 kHz
Coupling variation	0.1–0.2 (200%)	0.15–0.35 (233%)	0.13–0.22 (169.2%)	0.14–0.28 (200%)	0.08–0.2 (250%)	0.16–0.32 (200%)	0.21–0.36 (168.2%)	0.1–0.25 (250%)	0.1–0.4 (400%)
Fluctuation	10%	10%	10%	20%	20%	20%	10.6%	10%	5.98%
Output characteristic	Constant Voltage	Constant power	Constant Voltage	Constant power	Constant power	Constant power	Constant Voltage or Current	Constant power	Constant Power
Maximum power	3.5 kW	3.3 kW	3.5 kW	100 W	70 W	450 W	300 W	400 W	400 W
Efficiency	92.8%–90.7%	85%–94%	87.3%–94%	83.5%–87.5%	66%–73%	88.5%–92.6%	86%–94.8%	85.8%–91.7%	86.1%–94.3%

The fluctuation is defined as (maximum output – minimum output)/maximum output × 100%.

Besides, this work is not a specific design for the level of industrial products. The experimental prototype aims to verify the feasibility of the proposed approach, and the designed experimental setup does not yet reach the level of the commercial product. Suppose that the proposed method is used to develop a design for a particular application, in that case, researchers should redesign the system according to the design method of this work and practical design requirements.

Moreover, similar to [10], [11], [12], [13], and [14], the detuned circuit design will increase reactive power, which can be verified according to the phase angle between U_p and I_p from Fig. 6. Therefore, the proposed method is suitable in low-power applications, where steady and sufficient transfer power is the top priority with extensive coupling variations [10], such as lighting equipment and kitchen appliances [14], [17].

Finally, to show the superiority of the proposed method with high-misalignment tolerance, the performance of the proposed approach is compared with other methods, as presented in Table II. Compared with all the methods [7], [8], [9], [10], [11], [12], [13], [14], the output fluctuation of the proposed method is the lowest, only 5.98%, and the allowable coupling variation range is the largest, from 0.1 to 0.4. Besides, compared with the methods [7], [8], [9], [12], [13], [14], the transfer efficiency of this approach is also comparable and acceptable, and the efficiency is higher than that of [10] and [11]. Therefore, the antimisalignment ability of the proposed clamp circuit-based IPT system with a reconfigurable rectifier is significantly superior to the other methods.

IV. CONCLUSION

This letter has proposed a clamp circuit-based IPT system with a reconfigurable rectifier, owning high position tolerance. Complicated control or dedicated coil design is not required. The clamp circuit can automatically switch between conductive or nonconductive (including partly conductive) conditions, which creates two *P–k* curves with stable top regions. The reconfigurable rectifier can alter from FBM to HBM, transforming the equivalent ac load from one value to the other, thus creating another two *P–k* curves with stable regions. In this way, taking advantage of the four curves, this letter realizes nearly stable output power against an extensive coupling variation. The results validate the outstanding coupling-insensitive ability of the proposed approach, which is suitable for applications demanding high mobility while the dc load is relatively fixed.

REFERENCES

[1] Z. Zhang, H. Pang, A. Georgiadis, and C. Cecati, "Wireless power transfer—An overview," *IEEE Trans. Ind. Electron.*, vol. 66, no. 2, pp. 1044–1058, Feb. 2019.

[2] Y. Chen, S. He, B. Yang, S. Chen, Z. He, and R. Mai, "Reconfigurable rectifier-based detuned series-series compensated IPT system for anti-misalignment and efficiency improvement," *IEEE Trans. Power Electron.*, vol. 38, no. 2, pp. 2720–2729, Feb. 2023.

[3] K. Song et al., "Design of DD coil with high misalignment tolerance and low EMF emissions for wireless electric vehicle charging systems," *IEEE Trans. Power Electron.*, vol. 35, no. 9, pp. 9034–9045, Sep. 2020.

[4] J. Mai, Y. Wang, Y. Yao, M. Sun, and D. Xu, "High-misalignment-tolerant IPT systems with solenoid and double D pads," *IEEE Trans. Ind. Electron.*, vol. 69, no. 4, pp. 3527–3535, Apr. 2022.

[5] Y. Chen, R. Mai, Y. Zhang, M. Li, and Z. He, "Improving misalignment tolerance for IPT system using a third-coil," *IEEE Trans. Power Electron.*, vol. 34, no. 4, pp. 3009–3013, Apr. 2019.

[6] Y. Zhang, S. Chen, X. Li, and Y. Tang, "Design methodology of free-positioning nonoverlapping wireless charging for consumer electronics based on antiparallel windings," *IEEE Trans. Ind. Electron.*, vol. 69, no. 1, pp. 825–834, Jan. 2022.

[7] X. Qu, Y. Yao, D. Wang, S. Wong, and C. K. Tse, "A family of hybrid IPT topologies with near load-independent output and high tolerance to pad misalignment," *IEEE Trans. Power Electron.*, vol. 35, no. 7, pp. 6867–6877, Jul. 2020.

[8] L. Zhao, D. J. Thrimawithana, U. K. Madawala, P. Hu, and C. C. Mi, "A misalignment tolerant series-hybrid wireless EV charging system with integrated magnetics," *IEEE Trans. Power Electron.*, vol. 34, no. 2, pp. 1276–1285, Feb. 2019.

[9] Y. Chen et al., "A hybrid inductive power transfer system with misalignment tolerance using quadruple-D quadrature pads," *IEEE Trans. Power Electron.*, vol. 35, no. 6, pp. 6039–6049, 2020.

[10] H. Feng, A. Dayerizadeh, and S. M. Lukic, "A coupling-insensitive X-type IPT system for high position tolerance," *IEEE Trans. Ind. Electron.*, vol. 68, no. 8, pp. 6917–6926, Aug. 2021.

[11] H. Feng, T. Cai, S. Duan, X. Zhang, H. Hu, and J. Niu, "A dual-side-detuned series–series compensated resonant converter for wide charging region in a wireless power transfer system," *IEEE Trans. Ind. Electron.*, vol. 65, no. 3, pp. 2177–2188, Mar. 2018.

[12] H. Feng, T. Cai, S. Duan, J. Zhao, X. Zhang, and C. Chen, "An LCC-compensated resonant converter optimized for robust reaction to large coupling variation in dynamic wireless power transfer," *IEEE Trans. Ind. Electron.*, vol. 63, no. 10, pp. 6591–6601, Oct. 2016.

[13] J. Mai, Y. Wang, Y. Yao, and D. Xu, "Analysis and design of high-misalignment-tolerant compensation topologies with constant-current or constant-voltage output for IPT systems," *IEEE Trans. Power Electron.*, vol. 36, no. 3, pp. 2685–2695, Mar. 2021.

[14] Y. Chen et al., "Reconfigurable topology for IPT system maintaining stable transmission power over large coupling variation," *IEEE Trans. Power Electron.*, vol. 35, no. 5, pp. 4915–4924, May 2020.

[15] Z. Huang, G. Wang, J. Yu, and X. Qu, "A novel clamp coil assisted IPT battery charger with inherent CC-to-CV transition capability," *IEEE Trans. Power Electron.*, vol. 36, no. 8, pp. 8607–8611, Aug. 2021.

[16] S. Chen et al., "An operation mode selection method of dual-side bridge converters for efficiency optimization in inductive power transfer," *IEEE Trans. Power Electron.*, vol. 35, no. 10, pp. 9992–9997, Oct. 2020.

[17] M. Itraj and W. Ettes, "Topology study for an inductive power transmitter for cordless kitchen appliances," in *Proc. IEEE PELS Workshop Emerg. Technol., Wireless Power Transf.*, 2018, pp. 1–8.